Initial Characterization of Massive Multi-User MIMO Channels at 2.6 GHz in Indoor and Outdoor Environments

Flordelis, Jose; Gao, Xiang; Dahman, Ghassan; Tufvesson, Fredrik; Edfors, Ove

2015

EUROPEAN COOPERATION
IN THE FIELD OF SCIENTIFIC
AND TECHNICAL RESEARCH

IC1004 TD(15)W1023
Barcelona, Spain
October 14–15, 2015

EURO-COST

SOURCE: EIT, Dept. of Electrical and Information Technology,
Lund University,
Sweden

Initial Characterization of Massive Multi-User MIMO Channels at 2.6 GHz in Indoor and Outdoor Environments

Jose Flordelis, Xiang Gao, Ghassan Dahman, Ove Edfors and Fredrik Tufvesson
Dept. of Electrical and Information Technology
Lund University
Box 118
SE-221 00 Lund
SWEDEN
Phone: +46 46 2229179
Fax: +46 46 129948
Email: *firstname.lastname*@eit.lth.se

Initial Characterization of Massive Multi-User MIMO Channels at 2.6 GHz in Indoor and Outdoor Environments

Jose Flordelis, Xiang Gao, Ghassan Dahman, Ove Edfors and Fredrik Tufvesson

Dept. of Electrical and Information Technology, Lund University, Lund, Sweden
Email: *firstname.lastname*@eit.lth.se

***Abstract*—The channel properties have a large influence on user separability in massive multi-user multiple-input multiple-output (massive MIMO) systems. In this paper we present spatio-temporal characteristics obtained from massive MIMO channel measurements at 2.6 GHz. The results are based on data acquired in both indoor and outdoor scenarios where a base station (BS) equipped with 64 dual-polarized antenna elements communicates simultaneously with nine single-antenna users. In the outdoor scenarios the BS is placed at two rooftops with different heights and the users are confined to a five-meter diameter circle and move randomly at pedestrian speeds. In the indoor scenarios, the users are located close to each other in a lecture theater and the BS is placed at various locations in the room. We report on the observed distribution of the delay spreads and angular spreads. Furthermore, the multi-user performance in terms of singular value spread of the MU-MIMO channel is also reported. Finally, statistics of the coherence time and coherence bandwidth of the propagation channel in various scenarios are given. The results are important for the design and analysis of massive MIMO systems, as well as in the development of realistic massive MIMO channel models.**

***Keywords*—multi-user multiple-input multiple-output systems, MU-MIMO, massive MIMO, large-scale MIMO, MIMO channel measurements, spatial separation, time evolution, channel model, second-order moment.**

I. Introduction

Massive MIMO is an emerging communication technology promising order-of-magnitude improvements in data throughput, link reliability, range, and transmit-energy efficiency [1]–[4]. These benefits arise from leveraging the additional degrees of freedom provided by an excess of antenna elements at the BS side. A typical massive MIMO system can consist of one or more BSs equipped with many, $M = 100$, say, antenna elements serving K single-antenna users in the same time-frequency resource. K is in the order of 10 to 20 users, possibly more. Due to its potential to greatly increase spectral efficiency compared to today's systems, massive MIMO is considered as one of the main directions towards future 5G communication systems [5]–[7].

Several measurement campaigns have been conducted to study the performance of massive MIMO in real propagation environments. In [8]–[10], we reported outdoor massive MIMO channel measurements at 2.6 GHz with a linear array and a cylindrical array, both having 128 antenna elements. The investigations concluded that real propagation channels allow effective use of massive MIMO technology in the sense that a large fraction of the sum-rate capacity of MIMO channels with independent and identically distributed (i.i.d.) Rayleigh fading can be achieved in real propagation channels with linear precoding schemes. This is also shown in [11] for indoor BS measurements. In [12] massive MIMO channel measurements using a scalable antenna array consisting of up to 112 elements were reported. The results in [12] further support the conclusions drawn in [9]–[11] that theoretical gains of massive MIMO can be achieved in practice. More recent results in [13] indicate that the benefits of massive MIMO can be reaped even in the difficult scenario of a group of users located close to each other with line-of-sight (LOS) to the BS. Altogether, the combined set of published experimental results on massive MIMO elevates it from a mere theoretical concept to a practical technology.

In this paper we present spatio-temporal characteristics obtained from massive MIMO channel measurements at 2.6 GHz in various indoor and outdoor scenarios. During the measurements users are distributed with high density and located close to each other, possibly with many other passive users acting as scatterers or shadowing objects. Furthermore, the multi-user performance in terms of singular value spread of the MU-MIMO channel is also reported. Finally, statistics of the coherence time and coherence bandwidth of the propagation channel in various scenarios are given. The results are important for the design and analysis of massive MIMO systems, as well as in the development of realistic massive MIMO channel models.

II. Measurement Description

This section provides an overview of the scenarios chosen for the massive MIMO measurement campaigns, a description of the actual measurement environments and a short account of the measurement equipment.

A. Measurement Scenarios

In this work we consider two system scenarios identified in [14] as important for future 5G systems, namely "open exhibition" and "crowded auditorium". The main characteristics of these two scenarios are summarized in Tab. I and Tab. II (taken from [15]), respectively.

According to [14], open exhibition consists of outdoor-deployed (macro) BSs serving outdoor-located UEs. UEs are distributed randomly with high density and move at pedestrian speeds. UEs locations are in principle completely random, although some correlation may exist for both the UEs positions and the traffic patterns at specific times and/or locations.

One of the most important aspects to analyze and model is the user separability of closely spaced users, possibly with many other (passive) people being around acting as scatterers or shadowing objects and thus interacting with the nearby MS antenna. In this scenario it is important to include the effect of the user hand, the user body and the user antenna.

TABLE I. "Open exhibition" main characteristics. [15]

Parameter	Value
Propagation environment	Outdoor
Cell geometry / Size	Irregular, delimited geometry / Medium to large
UE distribution	Random, but clustered, with high density
UE speed	Up to 7 km/h
LOS/NLOS	Both
Shadow fading	Present
Channel model	COST2100
METIS relation	TC9 "Open air festival"
Examples	Outdoor conference center, crowded square

TABLE II. "Crowded auditorium" main characteristics. [15]

Parameter	Value
Propagation environment	Indoor
Cell geometry and size	Determined by scenario boundaries
UE distribution	Random, but clustered, with high density
UE speed	Mostly static, up to 3 km/h
LOS/NLOS	Both
Shadow fading	Not present
Channel model	COST2100
Examples	Indoor conference center, office, concert hall, indoor arena
METIS relation	TC1: "Virtual reality office", TC3 "Shopping mall", TC4: "Stadium"

From a measurement perspective, while still capturing the essential characteristics of the channel, we downscale the scenario to a group of a few users being located close to each other, with or without other people around, simultaneously communicating with a macro BS in LOS or NLOS. In our measurements we have 9 single-antenna users confined to a circle of 5 m diameter and describing random trajectories at pedestrian speeds while holding the MS in browse mode in front of their body with one hand. We consider two different positions of the BS, high- and low-roof, and several positions of the UE circle (UE sites), in both LOS and NLOS to the BS. The main characteristics of the outdoor measurement scenarios are summarized in Tab. III.

Crowded auditorium provides the indoor counterpart of the outdoor scenario described above. In this scenario both UEs and BSs are, respectively, located and deployed indoors. The UEs are randomly distributed with high density, possibly with correlated UEs positions and traffic patterns. The UEs are almost static in most cases and NLOS propagation conditions are expected. A subcase may be considered in which the UEs are static, placed at deterministic locations (e.g., seats in a concert hall) and channels contain LOS components.

Again, we capture the essential characteristics of this scenario by downscaling it to a case with a group of closely located indoor users in a lecture theater communicating with a BS mostly in LOS but with some obstructions. The users are seated regularly with and without other passive users around them acting as scatterers or shadowing objects. As opposed to the outdoor case we expect larger angular spreads due to more interaction with the indoor walls. Users hold the MS in browse mode in front of their bodies with one hand, all users facing the theater stage. Although the positions of the users are static, MSs describe random trajectories in front of each user's body at a speed of one revolution every 2 to 4 seconds. The purpose of the MS movements is to generate statistics of typical movements of MSs in a lecture theater. In our measurements we consider four BS locations and two different UE sites. The main characteristics of the indoor measurement scenarios are summarized in Tab. IV.

TABLE III. "Outdoor" measurements main characteristics.

Parameter	Value
Propagation environment	Outdoor
Carrier frequency	2.6 GHz
Cell geometry and size	5 m diameter circle
BS location	High-roof (BS 2) and low-roof (BS 1)
BS antenna height	23 m at BS 2, and 7 m at BS 1
UE distribution	Random, 9 active UEs and, optionally, up to 11 passive people
UE speed	Up to 0.5 m/s
UE location	LOS sites MS 1, MS 2, and NLOS sites MS 3, MS 4
LOS/NLOS	LOS or NLOS, depending on UE site
Shadow fading	Present
UE antenna height	160 cm
UE antenna grip	one-handed web-browsing
UE antenna tilt	45° from the vertical

B. Measurement Environment

In the outdoor case, measurements took place at the campus of Lund University, Lund, Sweden

TABLE IV. "INDOOR" MEASUREMENTS MAIN CHARACTERISTICS.

Parameter	Value
Propagation environment	Indoor
Carrier frequency	2.6 GHz
User distribution	Located at 4 rows of 5 adjacent seats (2.5×3.5 m^2)
BS antenna height	3.2 m
UE distribution	Deterministic, 9 active UEs and, optionally, 11 passive people
UE speed	UE antennas move in random trajectories in front of the user at low speed
LOS/NLOS	LOS with obstructions by room furniture and users seating nearby
UE antenna height	50 cm to 100 cm over the floor level, occasionally below furniture line
UE antenna grip	one-handed web-browsing
UE antenna tilt	Vertical, 45° downtilt

(55.711510 N, 13.210405 E), which can be described as a suburban environment having detached buildings with two to five floors and open areas with low vegetation and some trees. Fig. 1 shows an aerial photo of the measurement area. The BS antenna array was placed on the roof of the E-building, at two different levels: BS 1 on top of a two-floors roof (low-roof) and BS 2 on top of a five-floors roof (high-roof). The precise locations of BS 1 and BS 2 are given in Fig. 1. Several UE sites, labeled MS 1 to MS 4, were considered, with sites MS 1 and MS 2 having LOS conditions to the BS array, and sites MS 3 through MS 5 having NLOS conditions (see Fig. 1). At each UE site, we have a 5 m diameter circle and up to nine users moving inside it, representing a situation of high user density. During the measurements, users were holding the antennas inclining them at about 45°, so that we have both vertical and horizontal polarizations reaching the BS antenna array. Note that, since users were allowed to turn around, the LOS component to the BS can be blocked in some snapshots, by the user holding the antenna or by other users (see Fig. 2).

In the indoor case, measurements took place in lecture hall E:A. Lecture hall E:A has a picthed floor so that listeners in the rear are sat higher than those at the front and have LOS to the theater stage. Note, however, that handheld devices are typically held at or close to desk level and, thus, the LOS from the device to BS may at times be obstructed by nearby listeners or by room furniture. Fig. 3 shows a floor plan of lecture hall E:A. In the measurements, we consider four BS locations labeled BS 1 to BS 4, and two UE sites, labeled MS 1 and MS 2. All four BS locations are on the stage side of the lecture hall, with locations BS 1 and BS 2 sideways centered and locations BS 3 and BS 4 next to a corner. We note that, at locations BS 1 and BS 3, the BS antenna array is located at least one Rayleigh distance apart from walls and other interacting objects and, thus, wavefronts impinging on the BS array can be assumed plane. On the other hand, at locations BS 2 and BS 4, the BS antenna array is located next to one or two walls, as it might be the case in pratical

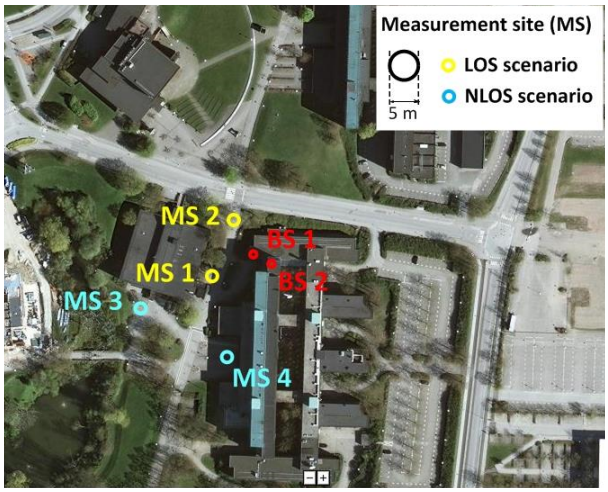

Fig. 1. Aerial photo of the outdoor measurement area. BS locations are indicated by labels BS 1 (low-roof) and BS 2 (high-roof). UE sites are labeled with MS 1 to MS 4, and the locations of the 5 m diameter circles have also been indicated. UE sites MS 1 and MS 2 have LOS condition to the BS, while MS 3 and MS 4 have NLOS.

(a) (b)

Fig. 2. (a) A user holding the MS user equipment antenna with an inclination of 45°. (b) Users moving randomly within the five-meter diameter circle at UE site MS 4.

BS indoor deployments. In all cases, the antenna array has been placed at a height of 3.2 m from the floor. UE sites MS 1 and MS 2 consist of a regular grid of four rows with five adjacent seats each, with an approximate area of 2.5×3.5 m^2. Site MS 1 comprises the center seats, whereas site MS 2 is located at the far corner from BS 3 and BS 4 and, in this sense, represents a worst case location. For each UE site, two different seat arrangements with nine seats each are considered, as illustrated in Fig. 3, where seats pertaining to each arrangement have been color-coded in red and blue. The rest of the seats are possibly occupied by passive users (crowd) acting as scatterers or shadowing objects (see Fig. 4). During the measurements, active users hold the terminal antenna either vertically of with a tilt of 45° relative to the vertical.

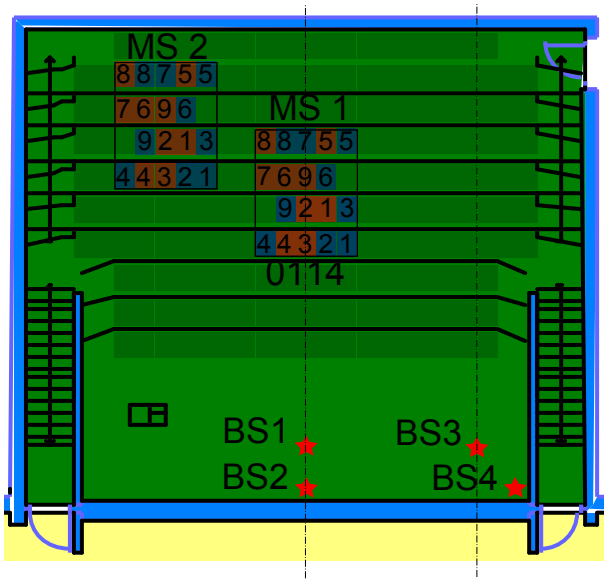

Fig. 3. Floorplan of the lecture theater used for "crowded auditorium" measurements. BS locations are indicated label BS 1 to BS 4. UE sites are labeled MS 1 (center) and MS 2 (back).

Fig. 4. Nine active users surrounded by eleven non-active users (crowd) at UE site MS 1. MS antennas are being held vertically and describe random trajectories.

C. Measurement Setup

Measurement campaigns for massive MIMO channel modeling were performed using a 128-port cylindrical antenna array at the BS side. The array consists of 64 dual-polarized patch antenna elements distributed in four rings stacked on top of each other. The spacing of adjacent elements is half a wavelength at 2.6 GHz. At the user side, we use nine single-polarized omni-directional antennas, of type SkyCross SMT-2TO6MB-A, acting as nine simultaneous users. Note that, although the antennas are vertically polarized and omni-directional in azimuth when measured without users, the radiation pattern and polarization including the users is more complex and is dependent on the exact position of antenna and users.

Measurements were recorded using the RUSK LUND MIMO channel sounder [16]. The sounder consists of a transmit unit (Tx) and a receive unit (Rx), which can operate untethered at separate locations. User antennas are connected to the transmit unit of RUSK LUND through optical fibers links. The transfer function of the radio channel is measured for all the Tx-Rx antenna pair combinations (SISO channels) providing a *snapshot* of the double-directional radio channel [17]. Snapshots are acquired at a fixed rate. The sampling rate f_s required for aliasing-free measurements depends on the mobility of the users, on the selected carrier frequency and on the environment, and must fulfill [18]

$$f_s \geq 2\nu_{\max}, \tag{1}$$

where $\nu_{\max} = f_c(v_{\max}/c_0)$ is the maximum Doppler shift of the channel, and $v_{\max}$, c_0 and f_0 are the maximum user speed, the speed of light in free space, and the carrier frequency, respectively. Tab. V summarizes the main configuration parameters.

TABLE V. RUSK LUND CONFIGURATION PARAMETERS.

Parameter	**Value** (indoor/outdoor)
Carrier frequency (f_c)	2.6 GHz
Bandwidth	40 MHz
Number of Tx-Rx channels	9*128
Number of subcarriers	129/257
Period of sounding signal (T_{sounding})	3.2/6.4 μs
Snapshot duration	$2 * 9 * 128 * T_{\text{sounding}}$
Number of snapshots	300
Measurement duration	17 s
Nominal output power	27 dBm

III. Data Processing for Channel Modeling

This section provides a brief description of the data processing methods utilized in this work.

From the RUSK LUND channel sounder we obtain a channel transfer function for each of the 9×128 Tx-Rx channels and 300 snapshots measured. Each such transfer function sounds the propagation channel at 257 (outdoor) or 129 (indoor) points equispaced within a 40 MHz bandwidth.

Next, directional analysis of the measurement data is accomplished by applying the SAGE algorithm [19]. The output from this step is a vector

$$\theta = [\tau_1, \phi_1, \theta_1, \alpha_1^{\mathrm{V}}, \alpha_1^{\mathrm{H}}, \ldots, \tau_P, \phi_P, \theta_P, \alpha_P^{\mathrm{V}}, \alpha_P^{\mathrm{H}}], \tag{2}$$

where τ_p, ϕ_p, θ_p, α_p^{V}, α_p^{H} are the delay, azimuth and elevation angle-of-arrival and amplitude of vertically and horizontally polarized components of the pth *multi-path component* (MPC), respectively, and P denotes the number of MPCs extracted from the channel observations. In our discussion, we let $P = 100$. SAGE is applied independently to each user and snapshot. Hence, we use the symbol $\theta_{k,n}$ to denote the MPCs corresponding to the propagation channel from user k to the BS antenna array at snapshot n.

The instantaneous delay spread S_τ of user k at snapshot n is computed as [18]

$$S_\tau = \sqrt{\sum_{p=1}^{P} \beta_p \tau_p^2 - T_\tau^2}, \tag{3}$$

where

$$T_\tau = \sum_{p=1}^{P} \beta_p \tau_p \tag{4}$$

is the mean delay and

$$\beta_p = \frac{|\alpha_p^{\mathrm{V}}|^2 + |\alpha_p^{\mathrm{H}}|^2}{\sum_{p=1}^{P} |\alpha_p^{\mathrm{V}}|^2 + |\alpha_p^{\mathrm{H}}|^2} \tag{5}$$

is the relative power of the pth MPC. Delays are measured in meters. Note that, for notational convenience, subindices k and n have been dropped in the expressions above.

The instantaneous mean azimuth angle-of-arrival T_ϕ and azimuth spread S_ϕ of user k at snapshot n are computed using expressions [18], [20]

$$T_\phi = \arg(\mu_\phi), \tag{6}$$

and

$$S_\phi = \cos^{-1}(|\mu_\phi|), \tag{7}$$

where

$$\mu_\phi = \sum_{p=1}^{P} \beta_p \exp(j\phi_p). \tag{8}$$

The mean elevation angle-of-arrival T_θ and elevation spread S_θ are computed in an analogous way. Note that, with these definitions, we have that $0 \leq S_\phi, S_\theta \leq 90°$.

The singular value spread and the normalized sum of squared singular values at snapshot n and subcarrier ℓ, which are used for the evaluation of system performance in Sec. IV, are computed directly from the channel transfer functions output by RUSK LUND as it is next explained. The following discussion applies to each time-frequency resource and, hence, we can drop subindices k and ℓ without loss of generality. Let $\mathbf{h}_k \in \mathbb{C}^{128\times 1}$ denote the propagation vector from user k to the BS antenna array and let $\mathbf{H} = [\mathbf{h}_1 \cdots \mathbf{h}_K]$ be a multi-user MIMO channel matrix with K the number of active users. Then, $\mathbf{H}$ admits a factorization of the form $\mathbf{H} = \mathbf{U}\mathbf{\Sigma}\mathbf{V}^{\mathrm{H}}$, where $\mathbf{U}$ and $\mathbf{V}$ are unitary matrices of suitable size and $\mathbf{\Sigma}$ is a diagonal matrix with elements $\sigma_1 \geq \ldots \geq \sigma_K \geq 0$. The singular value spread κ is defined as

$$\kappa = \frac{\sigma_1}{\sigma_K}, \tag{9}$$

and the normalized sum of squared singular values γ can be computed as

$$\gamma = \frac{1}{\sigma_1^2} \sum_{k=1}^{K} \sigma_k^2. \tag{10}$$

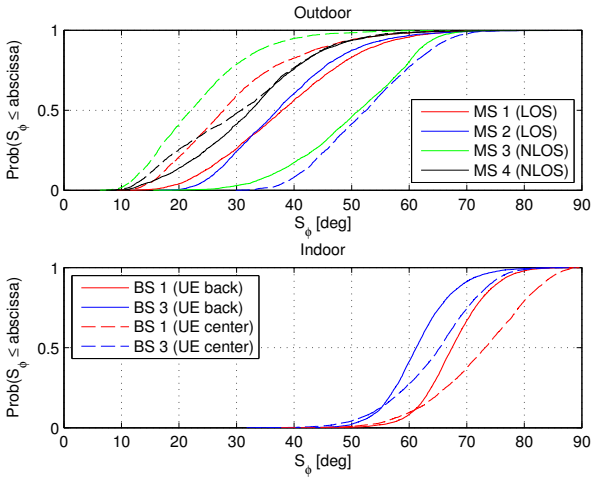

Fig. 5. Cumulative distribution of the azimuth angular spread at the BS in various outdoor (top) and indoor (bottom) scenarios. For the outdoor scenarios, plots for four UE sites, labeled MS 1–MS 4, and two BS positions, **high-roof** (in dashed line style) and **low-roof** (in solid line style) are shown. For the indoor scenarios, plots for two UE locations, back and center, and two BS positions, center (BS 1) and corner (BS 3), are shown.

IV. Results and Discussion

For the results reported in this section, only measurements without crowd have been considered. In a similar vein, no difference is made between seat arrangements (see Sec. II).

A. *Second-Order Moments*

In this section we look at the distribution of the second-order moments of the MIMO channel, i.e. delay spread and azimuth and elevation angular spreads at the BS. Fig. 5 shows the cumulative distribution of the azimuth angular spread for several outdoor and indoor measured scenarios.

In general, we observe larger azimuth angular spreads in indoor scenarios (median values between 60° to 75°) compared to outdoor ones (median values between 20° to 40°). This is due to more interaction with indoor walls and other scatterers in the room, which results in reflections arriving at the BS array from various directons. By contrast, the angular distribution of interacting objects in outdoor environments tends to be more sparse. As a result, more efficient use of multiple element antenna arrays (i.e. higher data rates) can be expected in indoor scenarios.

In fact, a detailed analysis of the measurement scenarios reveals that in the lecture theater there are two main directions of arrival, which correspond to (i) LOS from terminal antenna to BS array, and (ii) a strong reflection on the metal rails supporting the white boards at the back of the theater stage. By contrast, in outdoor scenarios, the BS array is reached mainly through only one direction (LOS direction, or direction of difraction

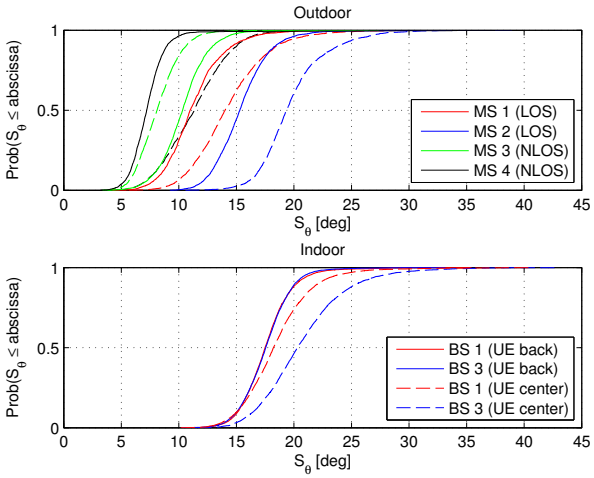

Fig. 6. Cumulative distribution of the elevation angular spread at the BS in various outdoor (top) and indoor (bottom) scenarios. For the outdoor scenarios, plots for four UE sites, labeled MS 1–MS 4, and two BS positions, **high-roof** (in dashed line style) and **low-roof** (in solid line style) are shown. For the indoor scenarios, plots for two UE locations, back and center, and two BS positions, center (BS 1) and corner (BS 3), are shown.

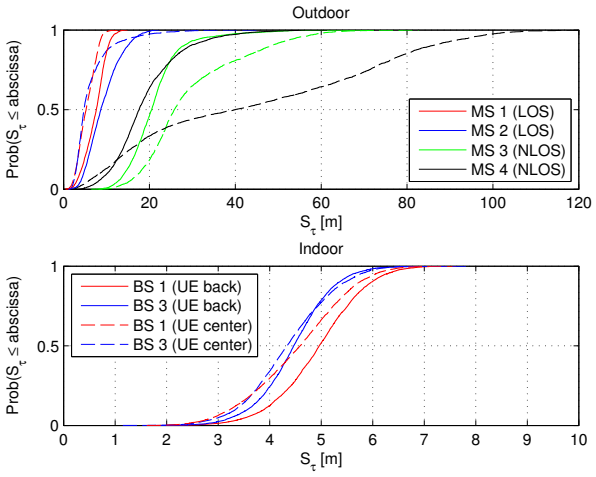

Fig. 7. Cumulative distribution of the delay spread of the propagation channel in various outdoor (top) and indoor (bottom) scenarios. For the outdoor scenarios, plots for four UE sites, labeled MS 1–MS 4, and two BS positions, **high-roof** (in dashed line style) and **low-roof** (in solid line style) are shown. For the indoor scenarios, plots for two UE locations, back and center, and two BS positions, center and corner, are shown.

around a building in NLOS). Note, however, than even in outdoor scenarios there might be situations in which several dominant directions of arrival exist. See, for example, curve MS2 for high-roof (dashed blue line in Fig. 5, top), which displays a median azimuth spread of 50°.

In indoor scenarios (Fig. 5, bottom), BS 1 (center) results in larger azimuth spreads than BS 3 (corner). In the same way, a larger azimuth spread is observed when users are located in the center sets of the lecture hall, rather than in the back seats. Intuitively, when MS and BS are located away from indoor walls, reflections from all directions are possible.

Fig. 6 shows the elevation angular spread at the BS for several outdoor and indoor measured scenarios. We see that, in all cases, spread in elevation is much smaller than the corresponding spread in azimuth, for both indoor and outdoor scenarios. In outdoor scenarios (Fig. 6, top), the array experiences larger elevation angular spread when it is mounted on a high-roof position than when it is mounted on a low-roof position. Similarly, scenarios with LOS display higher elevation spread than those with NLOS. Again, we observe that higher spreads are found in indoor environments (Fig. 6, bottom) compared to outdoor ones, also when the spread in elevation angular spread at the BS is considered.

Fig. 7 shows the delay spread for several outdoor and indoor measured scenarios. As expected, we observe that (i) the delay spread is larger in outdoor scenarios than in indoor ones, and (ii) in outdoor environments, the delay spread is larger in NLOS scenarios than in LOS ones.

B. *Multi-User Behavior*

So far, we have studied the second-order moments of the single-user MIMO channel. In this section, we consider the case in which several users, each with second-order moments distributed according to the laws introduced in Fig. 5 and Fig. 6, are located close to each other. The BS desires to serve these users in the same time-frequency resource and, hence, user data streams must be multiplexed in the spatial domain. In this case, it is the angular spread of the group of users that is of interest. The *g*roup angular spread is important for the design and analysis of massive MIMO communication schemes such as joint spatial division and multiplexing (JSDM) [21], [22], which relies in the idea of partitioning users into groups with similar second-order channel statistics.

In order to estimate the angular spread of a group of users we will assume that each user fills a rectangular area in the azimuth-elevation parameter space with sides and center given by the instantaneous angular spreads and mean angles, respectively, computed according to Sec. III. Fig. 8 illustrates this situation for the case of nine users located close to each other in various outdoor (top) and indoor scenarios (bottom).

We define the angular spread of a group of users as the union of the areas occupied by their respective rectangles. Intuitively, users with non-overlapping rectangles offer good angular separation and, hence, we expect the BS to be able to resolve them. Users with overlapping rectangles may be resolved if the group angular spread is "large enough"; that is, if the group angular spread covers, at least, as many "resolution

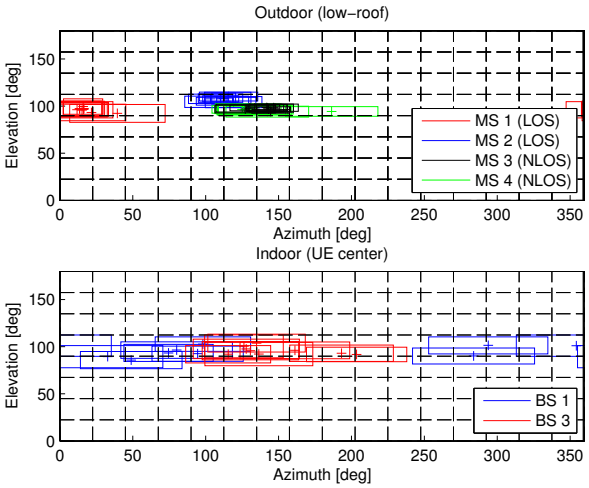

Fig. 8. Instantaneous power angle-of-arrival density of nine users located close to each other in outdoor (top) and indoor (bottom) scenarios, at one snapshot. For each user, instantaneous mean delays are marked as crosses. The overlaid grid indicates the resolution of the BS antenna array used during the measurements (see Sec. IV-D.)

bins" of the BS antenna array as there are users in the group.

If the union area introduced above is, as well, approximated by a rectangle, then the sides of the rectangle can be regarded as the *group* azimuth angular spread and *group* elevation angular spreads. Fig. 9 and Fig. 10 show the cumulative distributions of the so-defined azimuth and elevation group angular spread, respectively, corresponding to a group of eight users[1] located close to each other in various outdoor (top) and indoor (bottom) scenarios. Here, the same comments as for Fig. 5 and Fig. 6 apply. We note, however, that the group angular spread in both azimuth and elevation is considerably larger than the angular spread associated with each individual user. In general, as the distance between BS and the UE group shortens, UE centroids are seen by the BS at increasingly distinct directions and, hence, the group angular spread will increase.

C. System Performance

In this section we look at system performance in terms of the singular value spread and the normalized sum of squared singular values introduced in Sec. III. The singular value spread is often used as a proxy for favorable propagation conditions. Values of the singular value spread close to one indicate that user propagation vectors are nearly pairwise orthogonal and, hence, multiplexing of data to several users can be accomplished effectively. The normalized sum of squared singular values (10) tells us how dominant the largest singular value is. As opposed to the singular value spread, the

[1]In Fig. 9 and Fig. 10 we use eight rather than nine users since during the measurements of the high-roof outdoor scenarios only eight users were present.

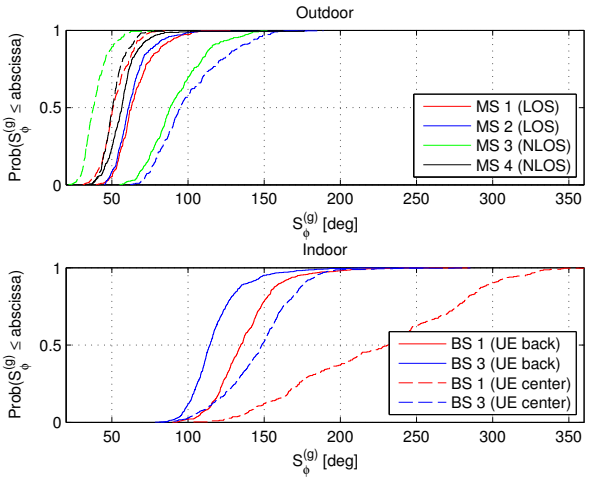

Fig. 9. Cumulative distribution of the azimuth group angular spread of a group of eight users located close to each other in various outdoor (top) and indoor (bottom) scenarios. In the outdoor scenarios, plots for four UE sites, labeled MS 1–MS 4, and two BS positions, **high-roof** (in dashed line style) and **low-roof** (in solid line style) are shown. In the indoor scenarios, plots for two UE locations, back and center, and two BS positions, center (BS 1) and corner (BS 3), are shown.

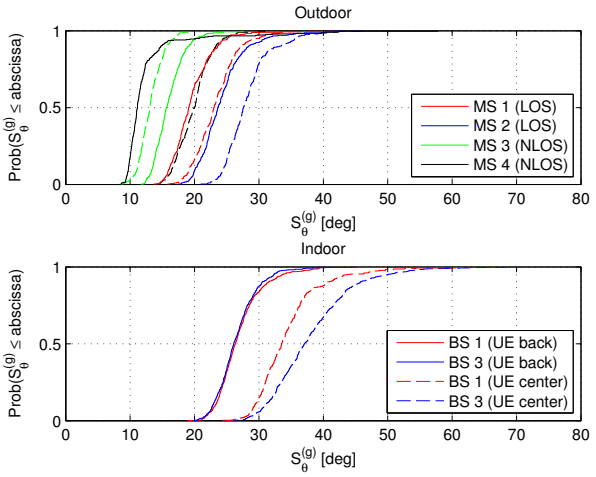

Fig. 10. Cumulative distribution of the elevation group angular spread of a group of eight users located close to each other in various outdoor (top) and indoor (bottom) scenarios. In the outdoor scenarios, plots for four UE sites, labeled MS 1–MS 4, and two BS positions, **high-roof** (in dashed line style) and **low-roof** (in solid line style) are shown. In the indoor scenarios, plots for two UE locations, back and center, and two BS positions, center (BS 1) and corner (BS 3), are shown.

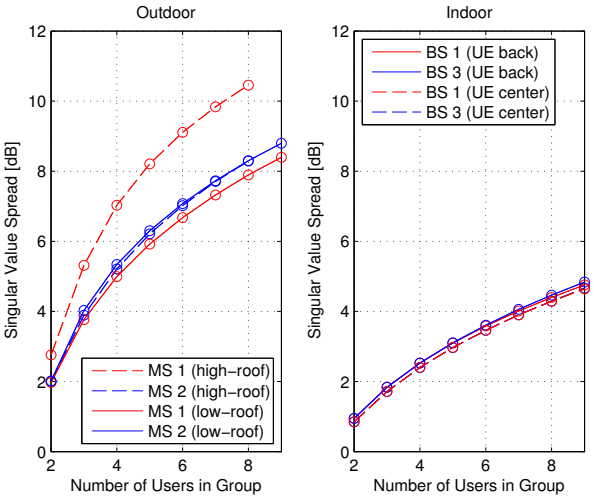

Fig. 11. Median of the singular value spread, in logarithmic units, when using 128 antenna ports at the BS in outdoor (left) and indoor (right) environments. In the outdoor environment, plots for two LOS UE sites, labeled MS 1 and MS 2, and two BS positions, **high-roof** (in dashed line style) and **low-roof** (in solid line style) are shown. In the indoor environment, plots for two UE locations, back and center, and two BS positions, center and corner, are shown.

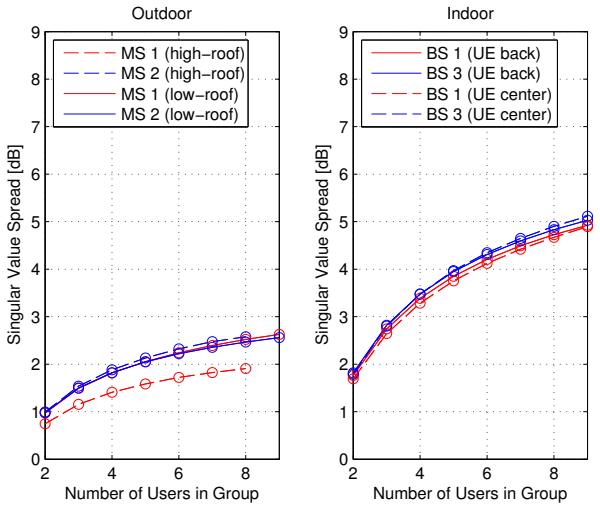

Fig. 12. Median of the normalized sum of squared singular values when using 128 antenna ports at the BS in outdoor (left) and indoor (right) environments. In the outdoor environment, plots for two LOS UE sites, labeled MS 1 and MS 2, and two BS positions, **high-roof** (in dashed line style) and **low-roof** (in solid line style) are shown. In the indoor environment, plots for two UE locations, back and center, and two BS positions, center and corner, are shown.

normalized sum of squared singular values makes use of all singular values of the multi-user channel matrix.

Fig. 11 and Fig. 12 show the median of the singular value spread and the median of the normalized sum of squared singular values as a function of the number of users for various outdoor (left) and indoor scenarios (right) in LOS. Except for UE site MS 1 when the BS antenna array is mounted on a high-roof, the median of the singular value spread is below 10 dB in outdoor scenarios, and below 5 dB in indoor scenarios. Hence, we may expect that all nine users can be served simultaneously in the same time-frequency resource at moderate signal-to-noise ratio (SNR) values.

Clearly, larger group angular spreads in indoor scenarios (see Fig. 9 and Fig. 10) result in lower singular value spreads than those in outdoor scenarios and, hence, in improved user separability. Within each group of indoor and outdoor scenarios, however, the relationship between group angular spread and singular value spread is not straightforward. As an example, consider UE site MS 1 in the lecture theater (center seats) and BS location BS 1. The corresponding curve (dashed red line in Fig. 9, bottom) shows a particularly large azimuth group angular spread, with a median value of about 240°. Nevertheless, all indoor scenarios show near identical properties in terms of the median of the singular value spread.

D. Group Angular Spread vs Singular Value Spread

Fig. 13 shows an interesting connection between user separability and group angular spread. We need first to define the normalized group angular spread $\bar{S}^{(g)}$ as the ratio between the group angular spread $S^{(g)}$ and the angular resolution of the BS antenna array $\xi_\phi \xi_\theta$. That is,

$$\bar{S}^{(g)} = \frac{S^{(g)}}{\xi_\phi \xi_\theta} \chi, \tag{11}$$

where the χ factor is 1 for single-polarized antenna ports and 2 for dual-polarized ones, were we assume that propagation is equally likely in bith polarization modes). In our measurements, $\xi_\phi = 22.5°$, $\xi_\theta \simeq 25°$, and $\chi = 2$. In Fig. 13, groups of K users, with $K = 2, \ldots, 9$, have been considered and, for each group, the median of $\bar{S}^{(g)}$ has been plotted against the median singular value spread of the group[2]. We observe that, for a given scenario, the singular value spread, when expressed in units of decibel, is approximately linearly related to the normalized group angular spread.

E. Temporal Behavior

Fig. 14 and Fig. 15 show the cumulative distribution of the 3-dB coherence time and 3-dB coherence bandwidth, respectively, of the SISO channels for various outdoor (top) and indoor (bottom) scenarios. These results are of interest for determining the maximum number of terminals that can be served by the BS [1]. The step-like shape in Fig. 14 is due to the relatively large sampling time; it provides, anyway, an indication of the experienced coherence time.

[2]The median of $\bar{S}^{(g)}$ has been computed over 300 snapshots, whereas the median of the singular value spread has been computed over 300 snashots and all subcarriers.

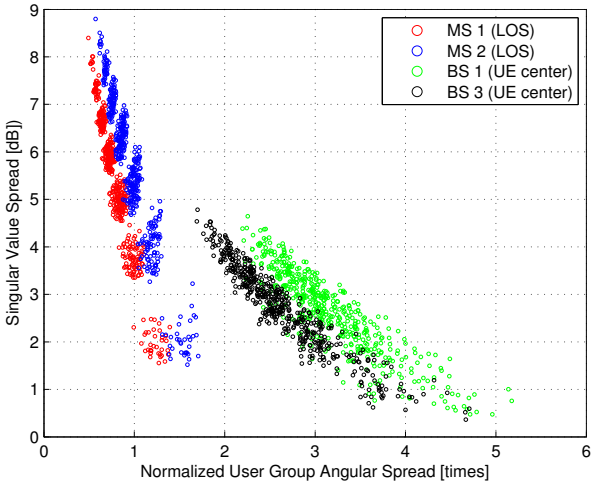

Fig. 13. Median of the normalized group angular spread versus median of the singular value spread for some indoor and outdoor scenarios. Low-roof outdoor scenarios with users at LOS sites MS 1 and MS 2 have been selected. For the indoor case, users are located at the center seats of the lecture theater and the BS array is located at BS 1 and BS 3.

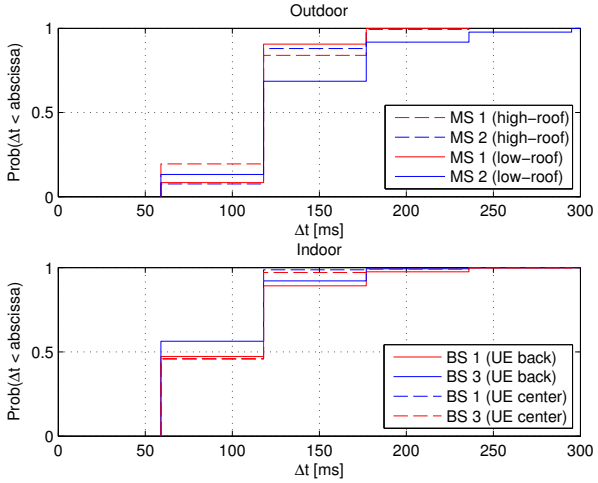

Fig. 14. Coherence time at 3-dB of SISO channels for some outdoor (top) and indoor scenarios (bottom). In the outdoor environment, plots for two LOS UE sites, labeled MS 1 and MS 2, and two BS positions, high-roof (in dashed line style) and low-roof (in solid line style) are shown. In the indoor environment, plots for two UE locations, back and center, and two BS positions, center and corner, are shown.

V. Summary and Conclusions

In this paper we have presented spatio-temporal characteristics of the massive MIMO channels obtained from channel measurements at 2.6 GHz in various indoor and outdoor scenarios. During the measurements users are distributed with high density and located close to each other, possibly with many other passive users acting as scatterers or shadowing objects. Different positions of the BS antenna array and of the user group have been considered. In particular, we have

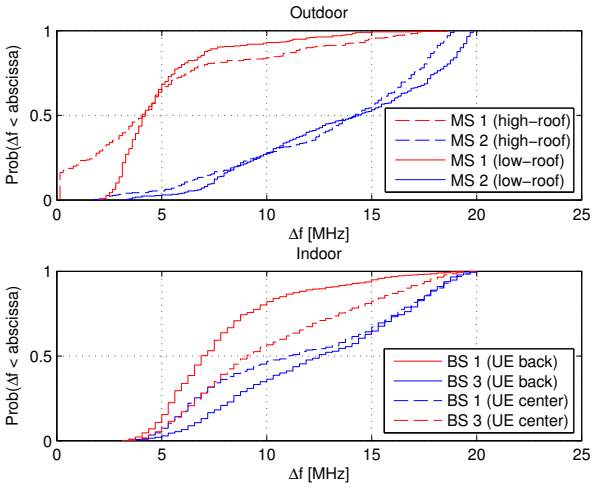

Fig. 15. Coherence bandwidth at 3-dB of SISO channels for some outdoor (top) and indoor scenarios (bottom). In the outdoor environment, plots for two LOS UE sites, labeled MS 1 and MS 2, and two BS positions, **high-roof** (in dashed line style) and **low-roof** (in solid line style) are shown. In the indoor environment, plots for two UE locations, back and center, and two BS positions, center and corner, are shown.

- Evaluated the distribution of the second-order moments of the propagation channel for various scenarios.
- Introduced the concept of group angular spread and provided its empirical distributions for groups of eight closely spaced users in various scenarios.
- Evaluated multi-user performance in terms of the singular value spread and normalized sum of squared singular values.
- Further, we have shown that a connection exists between group angular spread and singular value spread.
- Finally, we have given the empirical distributions of the coherence time and coherence bandwidth of the measured channel.

These results are important for the design and analysis of massive MIMO systems, as well as in the development of realistic massive MIMO channel models.

VI. Acknowledgements

The authors would like to acknowledge the financial support from ELLIIT - an Excellence Center at Linköping-Lund in Information Technology, and the Swedish Research Council (VR) as well as the Swedish Foundation for Strategic Research (SSF). This research has also received funding from the EU 7th Framework Programme under GA n° ICT-619086 (MAMMOET).

REFERENCES

[1] T. L. Marzetta, "Noncooperative cellular wireless with unlimited number of base station antennas," *IEEE Trans. Wireless Commun.*, vol. 9, pp. 3590–3600, Nov. 2010.

[2] F. Rusek, D. Persson, B. K. Lau, E. G. Larsson, T. L. Marzetta, O. Edfors, and F. Tufvesson, "Scaling up MIMO: Opportunities and challenges with very large arrays," *IEEE Signal Process. Mag.*, vol. 30, pp. 40–60, Jan. 2013.

[3] E. G. Larsson, F. Tufvesson, O. Edfors, and T. L. Marzetta, "Massive MIMO for next generation wireless systems," *IEEE Commun. Mag.*, vol. 52, pp. 186–195, Feb. 2014.

[4] H. Q. Ngo, E. G. Larsson, and T. L. Marzetta, "Energy and spectral efficiency of very large multiuser MIMO systems," *IEEE Trans. Wireless Commun.*, vol. 61, pp. 1436–1449, Apr. 2013.

[5] J. Andrews, S. Buzzi, C. Wan, S. Hanly, A. Lozano, A. Soong, and J. Zhang, "What will 5G be?," *IEEE J. Sel. Areas Commun.*, vol. 32, pp. 1065–1082, June 2014.

[6] F. Boccardi, R. Heath, A. Lozano, T. Marzetta, and P. Popovski, "Five disruptive techonology directions for 5G," *IEEE Commun. Mag.*, vol. 52, pp. 74–80, Feb. 2014.

[7] A. Osseiran, F. Boccardi, V. Braun, K. Kusume, P. Marsch, M. Maternia, O. Queseth, M. Schellmann, H. Schotten, H. Taoka, H. Tullberg, M. Uusitalo, B. Timus, and M. Fallgren, "Scenarios for 5G mobile and wireless communications: the vision of the METIS project," *IEEE Commun. Mag.*, vol. 52, pp. 26–35, May 2014.

[8] S. Payami and F. Tufvesson, "Channel measurements and analysis for very-large array systems at 2.6 GHz," in *Proc. EuCAP 2012 - 6th European Conf. in Ant. and Prop.*, pp. 433–437, Mar. 2012.

[9] X. Gao, F. Tufvesson, O. Edfors, and F. Rusek, "Measured propagation characteristics for very-large MIMO at 2.6 GHz," in *Proc. ASILOMAR 2013 - 46th Conf. on Sig., Syst. and Comput.*, pp. 295–299, Nov. 2012.

[10] X. Gao, O. Edfors, F. Rusek, and F. Tufvesson, "Massive MIMO in real propagation environments," *arXiv:1403.3376 [cs.IT], Submitted to IEEE Trans. Wireless Commun.*

[11] X. Gao, O. Edfors, F. Rusek, and F. Tufvesson, "Linear precoding performance in measured very-large MIMO channels," in *Proc. VTC 2011 Fall - IEEE 74th Vehicular Technology Conf.*, pp. 1–5, Sept. 2011.

[12] J. Hoydis, C. Hoek, T. Wild, and S. ten Brink, "Channel measurements for large antenna arrays," in *Proc. ISWCS 2012 - IEEE 9th Int. Symp. on Wireless Commun. Syst.*, vol. IT-29, pp. 811–815, Aug. 2012.

[13] J. Flordelis, X. Gao, G. Dahman, F. Rusek, O. Edfors, and F. Tufvesson, "Spatial separation of closely-spaced users in measured massive multi-user MIMO channels," in *Proc. ICC 2015 - IEEE Int. Conf. Commun.*, June forthcoming.

[14] E. Karipidis, J. Lorca, and E. Björnsson, "System scenarios and requirements specifications," tech. rep., MAMMOET, 2015.

[15] A. Bourdoux, C. Desset, L. van der Perre, G. Dahman, O. Edfors, J. Flordelis, X. Gao, C. Gustafson, F. Tufvesson, F. Harrysson, and J. Medbo, "MaMi channel characteristics: Measurement results," tech. rep., FP7 MAMMOET, July 2015.

[16] R. S. Thomä, D. Hampicke, A. Richter, G. Sommerkorn, A. Schneider, U. Trautwein, and W. Wirnitzer, "Identification of time-variant directional mobile radio channels," *IEEE Trans. Instrum. Meas.*, vol. 49, pp. 357–364, Apr. 2000.

[17] M. Steinbauer, A. F. Molisch, and E. Bonek, "The double-directional radio channel," *IEEE Trans. Antennas Propag.*, vol. 43, pp. 51–63, Aug. 2001.

[18] A. F. Molisch, *Wireless Communications*. New York: John Wiley & Sons, 2011.

[19] B. Fleury, M. Tschudin, R. Heddergott, D. Dalhaus, and K. Ingeman-Pedersen, "Channel parameter estimation in mobile radio environments using the sage algorithm," *IEEE J. Sel. Areas Commun.*, vol. 17, no. 3, pp. 434–450, 1999.

[20] B. Fleury, "First- and second-order characterization of direction dispersion and space selectivity in the radio channel," *IEEE Trans. Inf. Theory*, vol. 46, no. 6, pp. 2027–2044, 2000.

[21] A. Adhikary, N. Junyoung, A. Jae-Young, and G. Caire, "Joint spatial division and multiplexing — the large-scale array regime," *IEEE Trans. Inf. Theory*, vol. 59, pp. 6441–6463, June 2013.

[22] N. Junyoung, A. Adhikary, A. Jae-Young, and G. Caire, "Joint spatial division and multiplexing: Opportunistic beamforming, user grouping and simplified downlink scheduling," *IEEE J. Sel. Topics Signal Process.*, vol. 8, pp. 876–890, Mar. 2014.